Effect of initial conditions on secondary vortex structure in mixing layers

By J. H. Bell

1. Motivation and objectives

This report covers the final months of an experimental research project aimed at obtaining quantitative data on the behavior of the secondary vortex structure in a turbulent mixing layer at moderate Reynolds numbers ($\mathrm{Re}_\delta = 2.9 \times 10^4$). This project was terminated before all the contemplated measurements could be made, and data were obtained only on the spatially stationary part of the secondary structure. Nonetheless, these data reveal some interesting facets of mixing layer behavior, which are discussed in the following report.

It is now widely appreciated that the turbulent mixing layer can support a wide array of vortex structures. Indeed, it is known that mixing layer growth is dominated by the development and interaction of large-scale spanwise vortices (Ho & Huerre 1984). In addition, a second mixing layer structure, consisting of rows of "rib" vortices winding in between adjacent spanwise vortices, has also been revealed (Bernal & Roshko 1986, Lasheras & Choi 1988). The role which this secondary structure plays in mixing layer development is not yet clear. It was first reported in conjunction with "mixing transition" (Konrad 1977), and it has been speculated that there is a connection between the secondary structure and the sudden appearance of small scale fluctuations in the layer, which enhance mixing (Ho 1990). In addition, recent direct Navier-Stokes simulations (Moser & Rogers 1990) have shown that the spanwise structures can be strongly distorted by the rib vortices riding between them. Finally, experiments conducted by Nygaard & Glezer (1991) have shown that both the primary spanwise structures and the secondary vortices are simultaneously controllable to a high degree. These studies may eventually lead to a time when mixing layer behavior can be predicted and precisely controlled to suit the needs of a particular application.

Past investigations of the secondary structure in turbulent mixing layers have focussed almost exclusively on mixing layers originating from laminar initial conditions, i.e. the boundary layers on the splitter plate are laminar. To some extent, this is due to the inability of simulations to reach Reynolds numbers appropriate to turbulent initial conditions. Another reason, however, is that the secondary structure occurring within a mixing layer starting from laminar initial conditions is strikingly obvious and remarkably stable (Bernal & Roshko 1986). When the secondary structure is spatially stationary in this manner, its gross features can be easily resolved with relatively simple single-point, time-averaged velocity measurements. When such measurements are made on a cross-sectional grid through the mixing layer, the secondary structure takes on the appearance of a row of counter-rotating streamwise vortices, embedded within the layer. But this is not observed in mixing

layers where the splitter plate boundary layers are turbulent. No secondary vortex structure can be discerned with single-point, time-averaged measurements, indicating that the structure is either "jittering" in some way or that it is not present in the flow. The primary, spanwise structure, on the other hand, is believed to behave in the same manner regardless of initial conditions. This change in the behavior of the secondary structure is especially interesting in light of the slightly increased far-field spreading rate of mixing layers with laminar initial conditions versus those with turbulent initial conditions in the same facility (Browand & Latigo 1979, Bell & Mehta 1990a).

In order to gain a real understanding of the behavior of the secondary vortex structure, it is necessary to use measurement techniques which can detect this structure even when it is "jittering". In the absence of such techniques, however, a simpler approach might be to impose a spatially stationary secondary structure on a mixing layer originating from turbulent initial boundary layers. The structure which occurs naturally in mixing layers with laminar initial conditions is known to be triggered by small spanwise perturbations in the upstream boundary layers (Bell & Mehta 1989b). If spanwise perturbations could be used to fix the structure in an initially turbulent mixing layer, it would be possible to observe the behavior of the secondary structure in this flow with relatively simple techniques. The following sections describe the results, originally intended as a preliminary study, of an experiment on a mixing layer with different types of strong spanwise perturbations imposed at the origin.

2. Accomplishments

Data have been obtained on the development of a two stream mixing layer with four different sets of initial conditions. In all four cases, the velocity ratio was set to $\lambda = 0.25$, and the maximum Reynolds number achieved was $Re_\delta = 2.9 \times 10^4$. A rotatable crossed hot-wire probe was used to make single-point, time-averaged measurements in the mixing layers. The results for three cases were previously described in Bell (1989); the results for one case are new. This case also includes some runs at different velocities, as described later.

2.1 Experimental apparatus and techniques

All work was performed in the *Mixing Layer Wind Tunnel* located in the Fluid Mechanics Laboratory at the NASA Ames Research Center (Figure 1). The wind tunnel consists of two separate legs which are driven individually by centrifugal blowers connected to variable speed motors. The two streams are allowed to merge at the sharp edge of the tapered splitter plate. The facility is more fully described in Bell (1989) and further details of the mixing layer wind tunnel design and calibration are given by Bell & Mehta (1989a).

Measurements were made using a single rotatable cross-wire probe held on a 3-D traverse and linked to a fully automated data acquisition and reduction system controlled by a MicroVax II computer. Individual statistics for the baseline and vortex-generator cases were averaged over 5,000 samples obtained at a rate of 400

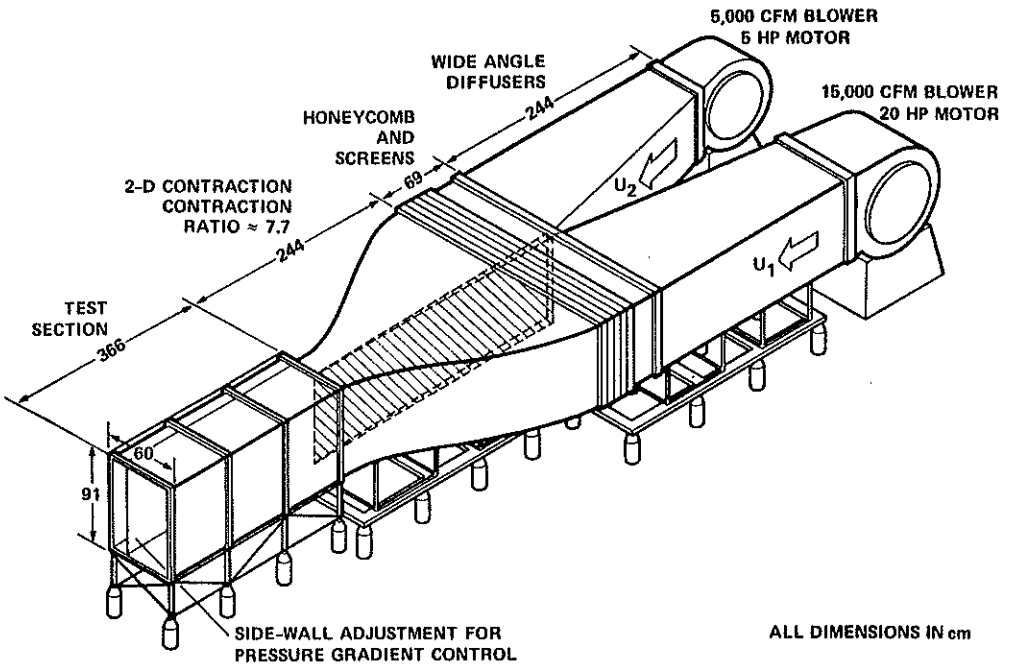

FIGURE 1. Mixing layer wind tunnel.

Hz. Upgraded equipment made available for the corrugated splitter plate case allowed 5,000 samples to be taken at a rate of 2.5 KHz.

Four cases are described in this report, each with differing initial conditions. These are sketched in figure 2, which shows the modifications made to the splitter plate in each case. In the *laminar* case, the splitter plate boundary layers were left undisturbed and remained in a laminar state. In the other three cases, round wire trips were installed on the splitter plate so as to produce fully-developed turbulent boundary layers at the splitter plate trailing edge. In the *tripped* case, no additional perturbations were imposed on the turbulent splitter plate boundary layers. In the remaining two cases, however, regular spanwise perturbations to the flow were also imposed. In the *vortex generator* case, a row of small vortex generators was installed on the high-speed side of the splitter plate. In the *corrugated* case, a cross-stream corrugation was added to the splitter plate trailing edge. The first three cases have been further described in Bell (1989) and Bell & Mehta (1990b). They are included here for comparison to the corrugated case, which is new. In all cases, the free-stream velocities were set at 15 m/s on one side and 9 m/s on the other, thus giving a mixing layer with velocity ratio, $U_2/U_1 = 0.6$, and $\lambda = 0.25$. The details of both the laminar and turbulent boundary layer properties near the splitter plate trailing edges are given below in table 1.

Table 1. Initial Boundary Layer Properties

Condition	U_e (m/s)	δ_{99} (mm)	θ (mm)	Re_θ	H	C_f $\times 10^3$
High-Speed Side, Laminar	15.0	4.0	0.53	525	2.52	0.7
Low-Speed Side, Laminar	9.0	4.4	0.61	362	2.24	0.9
High-Speed Side, Tripped	15.0	7.6	0.82	804	1.49	5.3
Low-Speed Side, Tripped	9.0	8.5	0.94	567	1.50	4.9

In the vortex generator case, streamwise vortices were injected into the mixing layer by a row of half-delta wing vortex generators, arranged as shown in figure 2. The vortex generator spacing was chosen to be comparable to the Kelvin-Helmholtz wavelength, and the semi-span was chosen to be approximately equal to the local boundary layer thickness.

In the corrugation case, a 2.5 cm plastic extension was attached to the end of the splitter plate. The extension was corrugated in the cross-stream direction, giving the splitter plate a three-dimensional trailing edge. The corrugation wavelength was 3.8 cm, and the amplitude increased from zero to 1.3 cm over a 2.5 cm distance. Since each full cycle of the corrugation would produce a pair of opposite-signed regions of cross-stream vorticity, the wavelength was chosen to be roughly twice the Kelvin-Helmholtz wavelength; the amplitude was chosen to be close to the local boundary layer thickness.

Data were obtained in the XY- and XZ-planes with a cross-wire probe at eight streamwise stations for each case. In the cases with turbulent initial boundary layers, the last station is $3050\theta_1$ downstream of the trailing edge. At each station, data were obtained in a cross-sectional plane which typically extended over 20 points in the cross-stream direction, and 60 points in the spanwise direction. The spanwise extent of each cross-sectional plane ranged from three to ten mixing layer thicknesses, depending on the streamwise location. The global properties presented below were *spanwise-averaged* for all cases. The measurements of U, W and $\overline{u'w'}$ were corrected for mean streamwise velocity gradient ($\partial U/\partial Y$) effects as described in Bell & Mehta (1989b). The streamwise component of mean vorticity ($\omega_x = \partial W/\partial Y - \partial V/\partial Z$) was computed using the central difference method. The overall circulation was defined as the surface integral of the streamwise vorticity over the cross-flow plane with vorticity levels less than 10% of the maximum value being set to zero in order to provide immunity from "noise".

2.2 Results and Discussion

The differing initial conditions result in considerable differences in the growth rates and turbulence levels, not only in the near-field but extending to the far downstream as well. Figure 3 shows the mixing layer thickness, δ, determined by fitting the mean velocity profile to an error function profile shape, for all four cases. All four cases attain linear growth in the far-field, but with striking differences in both near- and far-field growth rates. In the near-field, the perturbed cases grow

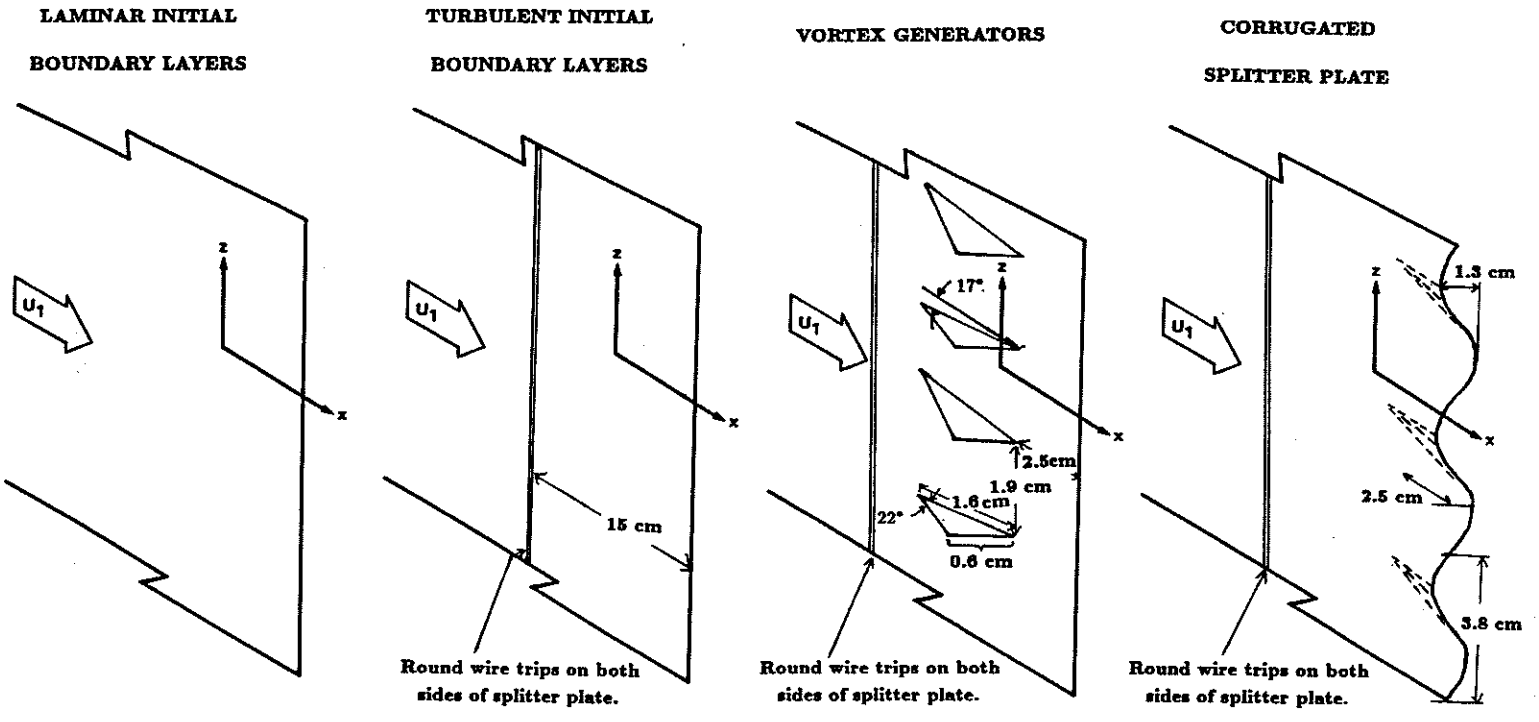

FIGURE 2. Sketches of the splitter plate trailing edge configurations for the four cases. Views are of the high-speed side of the splitter plate.

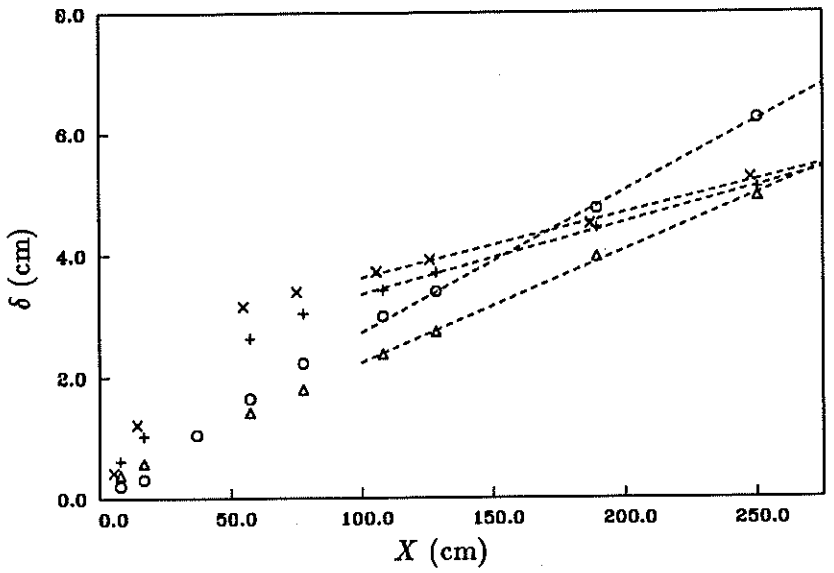

FIGURE 3. Mixing layer thickness, δ, vs. streamwise distance, X. The dashed lines are best fits to the far field data, and the far field growth rates are listed below: ○ laminar case $d\delta/dx = 0.023$, △ tripped case $d\delta/dx = 0.019$, + vortex generator case $d\delta/dx = 0.012$, × corrugated case $d\delta/dx = 0.011$.

much more rapidly than the unperturbed cases, but their far-field growth rates are much reduced. The tripped case growth rate in the linear region is $d\delta/dx = 0.023$, which is close to the value typically observed for mixing layers with $\lambda = .25$ (Rodi 1975). However, the far-field growth rate for the laminar case is 28% higher than that for the tripped case, and that for the vortex generator and corrugated splitter plate cases are 33% and 39% lower, respectively. Despite the difference in the perturbations, the vortex generator and corrugated cases both grow at nearly the same rate.

Since the mixing layer growth rates are so drastically affected by the perturbations at the origin, the Reynolds stresses levels might be expected to show a comparable effect. This is indeed the case, as shown in figure 4, which plots the streamwise development of the peak turbulent kinetic energy, $\overline{q^2}_{max}$. Both the laminar and tripped cases asymptote to about the same constant level beyond $X \sim 125$ cm. By the same streamwise location, the perturbed cases have achieved a significantly lower constant level (Which is nearly identical for the two cases.). In the near-field, the laminar case displays the classically observed "overshoot" in turbulence intensity, before dropping down to the asymptotic level. This overshoot is most likely due to the coherent passage of spanwise vortex structures. The overshoot seen in the perturbed cases is due to the generation of very high turbulence levels as the mixing layer is strained by the strong streamwise vortices induced by the perturbations. In the laminar case, the overshoot is made up of very strong fluctuations at the Kelvin-Helmholtz frequency, while in the perturbed cases it is much more broadband. The

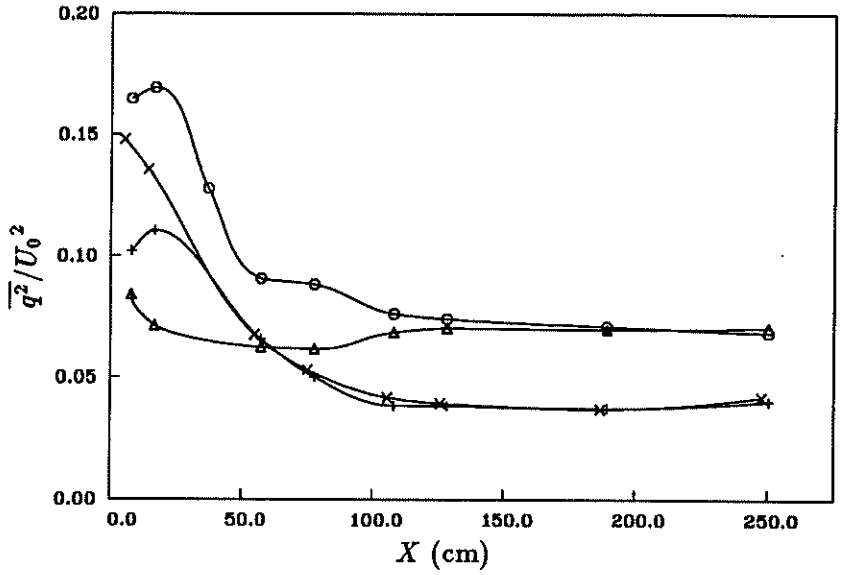

FIGURE 4. Peak level of $\overline{q^2}/{U_0}^2$, or twice the turbulent kinetic energy vs. streamwise distance,, X, for the four cases. ○ laminar case, △ tripped case, + vortex generator case, × corrugated case.

very slight overshoot in the turbulent case is due to the high turbulence levels generated in the wake behind the splitter plate.

In a self-similar mixing layer, it is possible to relate the peak level of primary shear stress, $(\overline{u'v'})_{max}$, to the mixing layer growth rate, $d\delta/dx$, and the velocity ratio parameter λ. The relation that evolves from the analysis given by Townsend (1976), is:

$$-\frac{\overline{u'v'}_{max}}{U_0^2} = 0.141\frac{d\delta}{dx}\frac{1}{\lambda}$$

This relationship is used to calculate $(\overline{u'v'})_{max}$ for each case. The results are compared with the measured values of $(\overline{u'v'})_{max}$, below in table 2.

Table 2. Measured and Calculated $(\overline{u'v'})_{max}$

$(\overline{u'v'})_{max}$	Laminar	Tripped	Vortex Generators	Corrugated Splitter Plate
Measured	0.011	0.011	0.0061	0.0065
Calculated	0.013	0.010	0.0067	0.0060

With the exception of the laminar case, the measured and calculated values of $\overline{u'v'}_{max}$ agree to within approximately 10%. The poor agreement in the laminar case suggests that this flow has possibly not reached a fully self-similar state, in spite of other indications that it has. The perturbed cases, on the other hand, behave in a manner consistent with the assumption of self-similarity, despite their abnormally low growth rates. The question which then arises is how far downstream this lowered

growth rate persists. In the present facility, measurements downstream of $X = 250.3$ cm, or $3050\theta_1$, are beginning to show the effects of sidewall interference. In order to effectively extend measurements farther downstream, data were taken for the corrugated case at different operating conditions.

First, the flow velocity on both sides was doubled, effectively doubling Re_x. This change had the effect of increasing the growth rate to $d\delta/dx = 0.013$, and increasing $\overline{u'v'}_{max}$ proportionately, to 0.0071. Second, the high speed side velocity was increased to 30 m/s, while the low speed side velocity remained at 9 m/s, giving $\lambda = 0.54$. This had the effect of increasing the velocity difference relative to the convection velocity. Thus, it was expected that the same physical distance downstream would correspond to a greater number of pairings of the spanwise structures, i.e., the mixing layer would be dynamically "older". In this case, $d\delta/dx$ was increased to 0.034, while the measured $\overline{u'v'}_{max}$ was 0.0069. If the mixing layer were self-similar, $\overline{u'v'}_{max} = .0088$ would be expected. However, it is clear that the growth rate and turbulence levels in this case are still much lower than would be expected from previous studies of turbulent mixing layers.

Contour plots of various mixing layer properties show a considerable difference in the near-field evolution of the four cases. Figure 5 shows contours of mean streamwise velocity at $X = 17$ cm. This station is fairly close to the splitter plate, and the distortion of the U^* distribution in to the presence of strong streamwise and cross-stream vorticity can be clearly observed in all but the tripped cases. The distortion is quite severe in the vortex generator and corrugated cases, especially so in the later because of the bending of the mixing layer by the strong cross-stream vorticity in this case. Turbulence distributions in the mixing layer are similarly affected, as seen in figure 6, which shows contour plots of $\overline{q^2}/{U_0}^2$ at the same location. The streamwise vortices produce isolated regions of high turbulence. In the laminar case, these tend to be lost in the background of the high fluctuation levels produced by the organized passage of the spanwise vortices. In the vortex generator and corrugated cases, especially high turbulence is found between the streamwise vortices, where the vortex-induced thinning of the mixing layer has increased the mean shear dramatically.

The mean streamwise vorticity contours show the most marked difference between the four cases. In the laminar case (figure 7a), an irregular row of $8-10$ streamwise vortices of varying strengths can be observed. In contrast, the tripped case (figure 7b) has a much lower level of vorticity in an irregular pattern, not at all suggestive of concentrated streamwise vortices. In the vortex generator and corrugated cases, a single row of 7 round, well-defined counter-rotating vortices are clearly observed. The variation in vortex strengths is much smaller than in the laminar case. The spacing between the vortices in the perturbed cases is approximately 2 cm, the same as the wavelength of the original spanwise disturbance. The mean streamwise vorticity is strongest at the first measurement station ($X = 8$ cm), and its effects on the other flow quantities are greatest at this location.

The behavior of the streamwise vorticity, in the three cases for which this quantity is significant, is presented in figure 8. The peak vorticity and circulation data

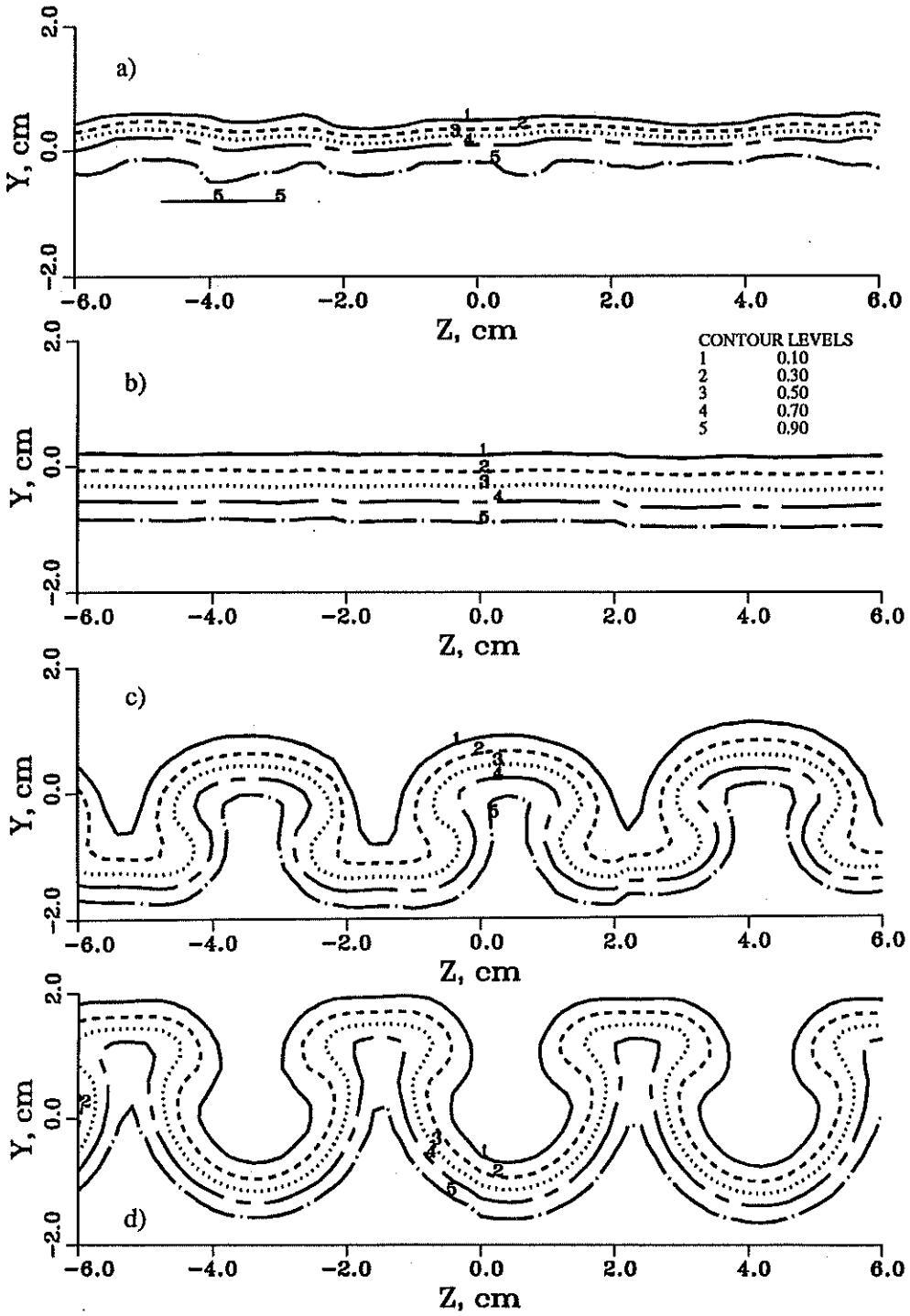

FIGURE 5. Contours of mean streamwise velocity U/U_0 at $X = 17$ cm. a) laminar case, b) tripped case, c) vortex generator case, d) corrugated case.

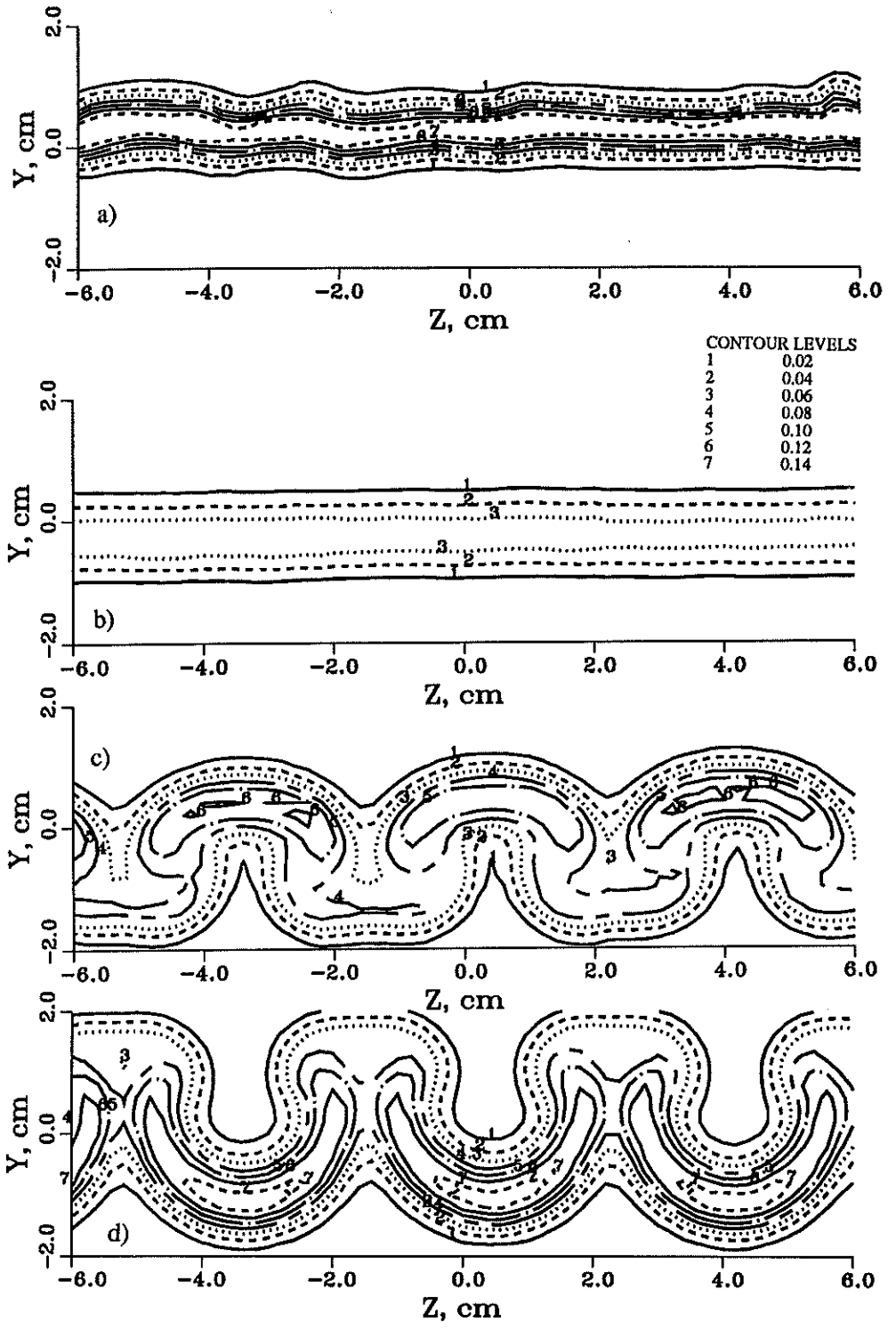

FIGURE 6. Contours of turbulent kinetic energy $\overline{q^2}/{U_0}^2$ at $X = 17$ cm. a) laminar case, b) tripped case, c) vortex generator case, d) corrugated case.

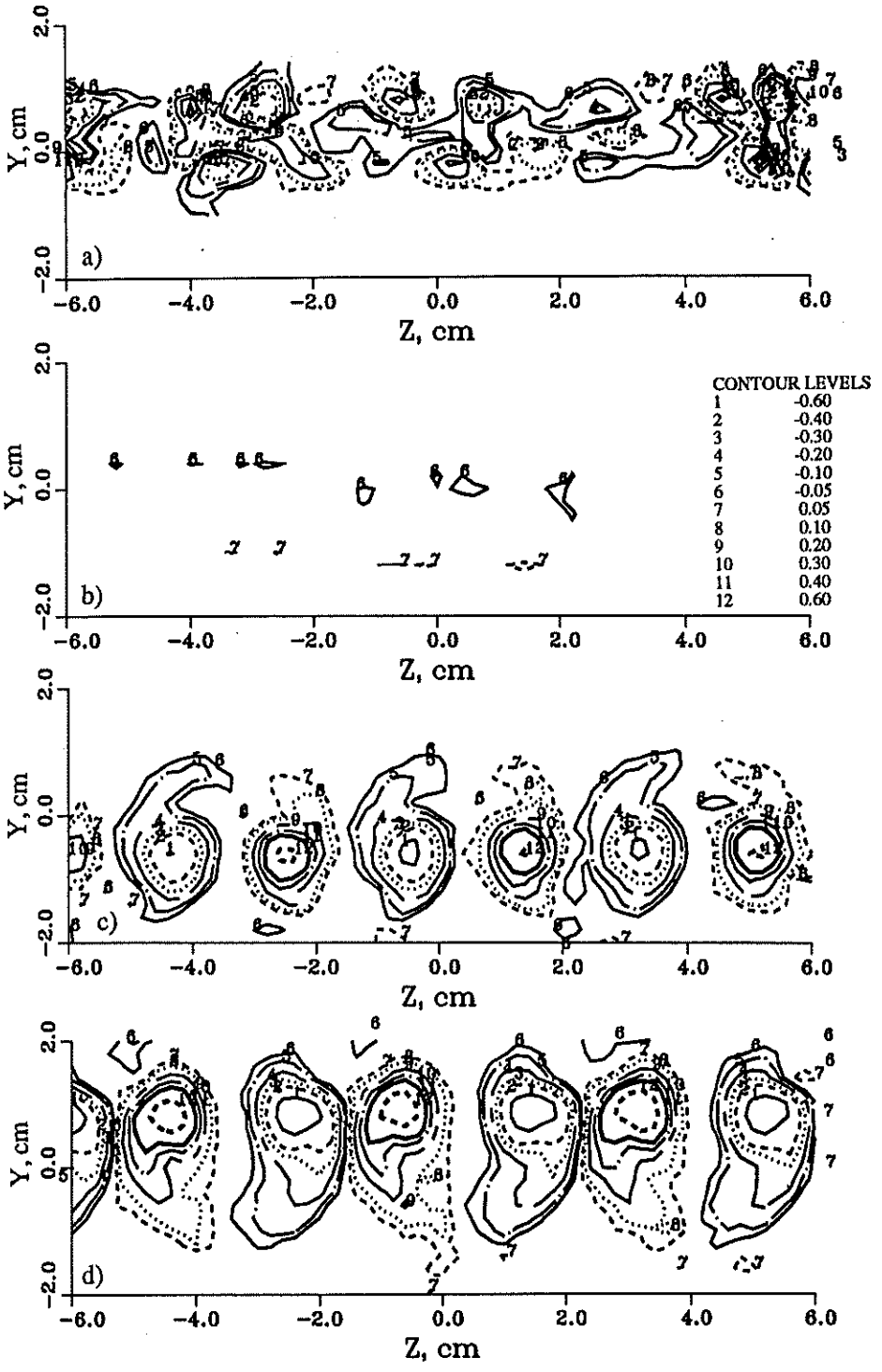

FIGURE 7. Contours of mean streamwise vorticity Ω_x/U_0 (cm^{-1}) at $X = 17$ cm. a) laminar case, b) tripped case, c) vortex generator case, d) corrugated case.

presented in figure 8 are left unnormalized. This is done because the most appropriate normalizing parameters — the initial strength and circulation of the spanwise structures — can only be estimated in the present study. Mean spanwise vorticity, $\Omega_z = (\frac{\partial V}{\partial x} - \frac{\partial U}{\partial y})$ was estimated by assuming that the $\frac{\partial V}{\partial y}$ term is negligible. Spanwise vortex circulation was estimated using an initial streamwise wavelength determined by the convection velocity and the measured natural frequency of the mixing layer. For the three cases, the estimated values of spanwise vorticity at the first measurement station are as follows. Laminar case: $\Omega_{z_{max}} = 1400\ s^{-1}$ and $\Gamma_z = 0.11\ m^2/s$, vortex generator case: $\Omega_{z_{max}} = 1100\ s^{-1}$ and $\Gamma_z = 0.11\ m^2/s$, corrugated case: $\Omega_{z_{max}} = 920\ s^{-1}$ and $\Gamma_z = 0.11\ m^2/s$. In the latter two cases, the estimates are made more uncertain by the highly distorted state of the mixing layer and the lack of a clearly observable natural frequency.

The streamwise development of the peak mean vorticity for the three cases is presented on a log-log scale in figure 8a. The peak vorticity values tend to fall along a straight line on this scale, indicating a power-law decay rate. The vortex generator case has the highest initial mean vorticity level, but also the fastest decay rate; dropping as roughly $1/X^{1.8}$. The vorticity decay rate for the laminar case is approximately $1/X^{1.5}$, and for the corrugated case, roughly $1/X^{1.6}$. As noted previously, these values reflect only the decay of the spatially stationary part of the secondary structure. It is possible that the structure is actually maintaining its strength, but "jittering" with increasing amplitude as it moves downstream.

The secondary vortex structure contains both streamwise and cross-stream vorticity. It is possible to estimate the latter by neglecting the $\frac{\partial W}{\partial x}$ term; thus $\Omega_y \cong \frac{\partial U}{\partial z}$. The ratio of streamwise to cross-stream vorticity at a given station gives some indication of the orientation of the secondary structure. This ratio, plotted in figure 8b, is initially very different for the three cases. In the laminar case, the developing secondary structure only gradually begins to kink the mixing layer, resulting in a very high Ω_x/Ω_y ratio initially. In the corrugated case, the high level of cross-stream vorticity imposed by the corrugations produces a much lower Ω_x/Ω_y ratio. Further downstream, Ω_x/Ω_y collapses to approximately the same value for all three cases, suggesting that the secondary structure is behaving in a similar fashion in all three flows, despite differences at the origin.

Plots of the vortex circulation (Figure 8c), however, show very different behavior for the three cases. The laminar case vortex circulation shows a very slow decrease, with a small intermediate peak at $X \sim 60$ cm — this was associated with the change in scale of the streamwise vortex structure (described below). However, the vortex generator case shows a relatively fast linear decay and by $X \sim 125$ cm, the level is comparable to that of the naturally occurring vortices. In the corrugated case, the circulation at the first two stations is quite high; it then drops to a level close to that of the vortex generator case. This result is surprising, since the peak vorticity of the corrugated case at the first station is lower than that for the vortex generator case. Evidently, the corrugations produce relatively diffuse, large-scale streamwise vortices which the mixing layer cannot support, and these decay rapidly.

The mean spacing of the streamwise vortices can be easily found by counting the

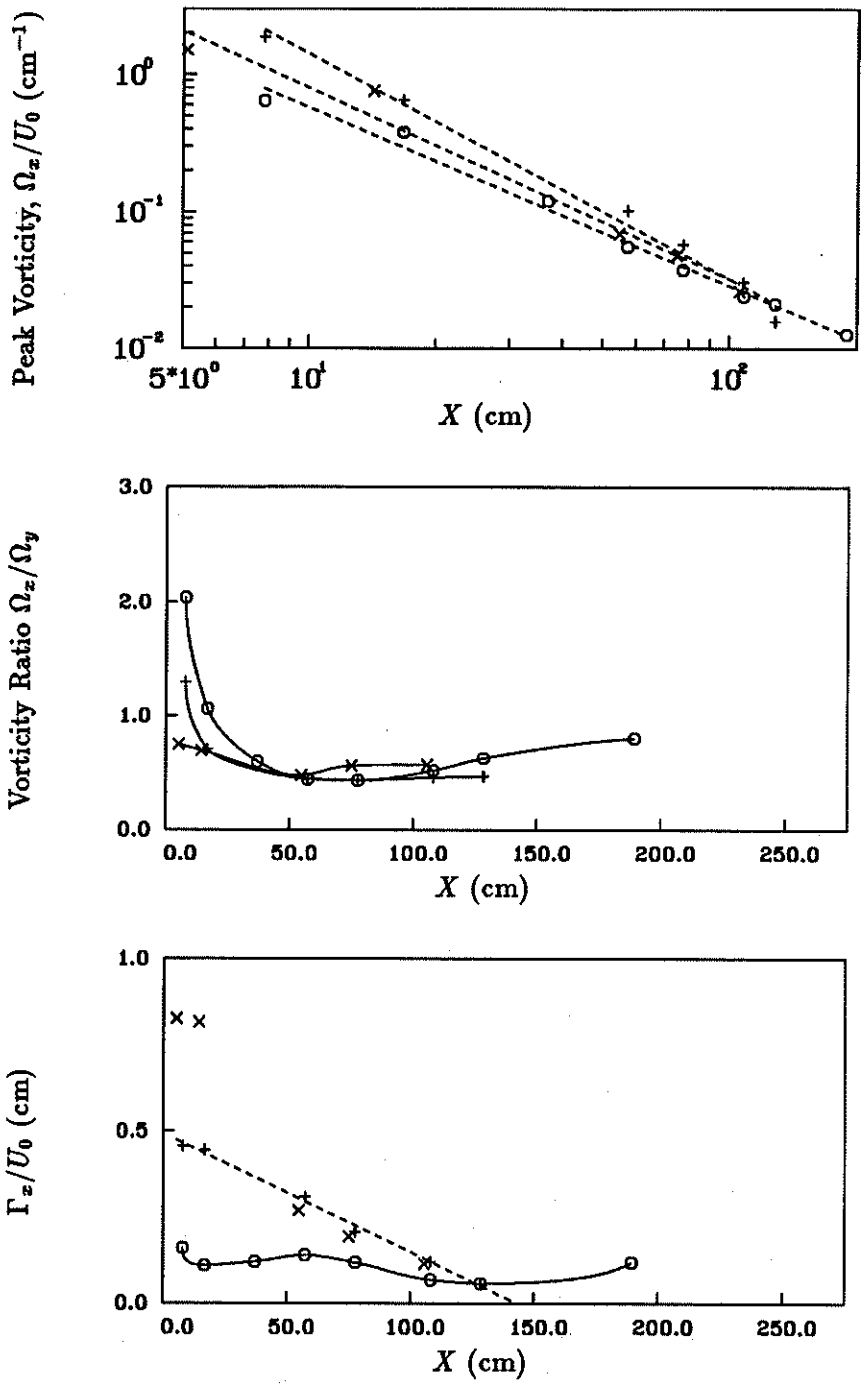

FIGURE 8a-c. Mean streamwise vorticity (Ω_z/U_0 cm^{-1}) properties for laminar and perturbed cases. ○ laminar case, + vortex generator case, × corrugated case. a) Peak streamwise vorticity vs X, log-log scale, b) Ratio of streamwise to cross-stream vorticity, Ω_z/Ω_y, c) Streamwise vortex circulation vs X.

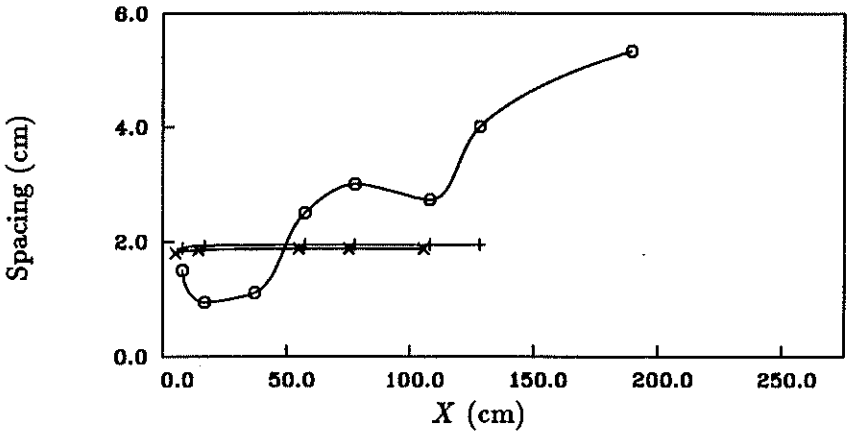

FIGURE 8d. Mean streamwise vortex spacing vs X, for laminar and perturbed cases. ◯ laminar case, + vortex generator case, × corrugated case.

number of vortices present at each station. The vortex spacing in the laminar case increases in a step-wise fashion, scaling approximately as the mixing layer vorticity thickness (Fig. 8d). On the other hand, the spacing for the vortex generator and corrugated cases is *constant* within the measurement domain. This may simply be due to the fact that the injected vortices are of equal strength and spacing, unlike the naturally occurring structures, and so there is no tendency for self-induced motion. Another possibility, related to the pairing of the *spanwise* structures, is discussed below.

3. Conclusions

The imposition of strong spanwise perturbations at the origin of a mixing layer produces a well-defined secondary vortex structure. The effects of this structure are striking. The initial ($X \leq 60$ cm) growth rate is increased significantly, most likely due to the extra entrainment provided by the streamwise structures. However, the growth rate further downstream ($X \geq 100$ cm) is reduced drastically over the unperturbed cases with either laminar or turbulent splitter plate boundary layers. These effects are essentially independent of the means used to impose the spanwise perturbations (either vortex generators or a corrugated end to the splitter plate). The region of reduced growth and turbulence levels extends very far downstream — at least 3000 times θ_1, the momentum thickness of the high-speed side splitter plate boundary layer. In addition, experiments in the corrugated case indicate that the region may extend more than twice this far downstream. In the region of reduced growth, the mixing layer gives every indication of having reached a self-similar state.

A possible explanation for this change can be made by postulating that the strong initial secondary vortex structure affects the pairing of the spanwise vortices. Most of the growth of a mixing layer occurs due to entrainment during the pairing process of the nominally two-dimensional spanwise vortical structures (Sandham *et al.* 1988). If the spanwise structures were altered so as to reduce the pairing rate,

entrainment by the mixing layer, and thus its growth rate, would be decreased. The naturally occurring streamwise vorticity in the laminar case first appears in the regions of maximum extensional strain, in the braid region. The two structures become interlaced in such a way that, in flow-visualization studies, it appears that the only effect of the secondary structure on the spanwise vortices is to produce a regular, gentle undulation in the latter (Lasheras *et al.* 1986). Therefore, the entrainment due to the spanwise structures proceeds undisturbed; total growth may in fact be enhanced by the additional entrainment in the braids due to the secondary structure. However, the injected vorticity in the vortex generator and corrugated cases imposes its own pattern on the spanwise structures, as indicated by the gross distortions in the mean velocity contours. It is possible that this changes the pairing process, reducing the pairing rate. In the near-field, entrainment by the secondary structure more than makes up for this deficit. However, entrainment due to the rib vortices decreases much faster than the spanwise structure recovers, so the overall entrainment rate is reduced, and hence the growth rate of the mixing layer drops. This hypothesis is also consistent with differences noted in the behavior of the streamwise vortices in the three cases. Previous investigations have suggested that the scale change in the streamwise vortices occurs during the pairing of the spanwise rollers (Jimenez *et al.* 1985, Bell & Mehta 1989b). A scale change is not observed in the vortex generator or corrugated cases, but the behavior of the vorticity ratio, Ω_x/Ω_y, suggests that the secondary structure achieves the same state in all three cases. The most reasonable explanation, then, is that the lack of a scale change in the vortex generator and corrugated cases indicates that the pairing of the spanwise rollers has been suppressed.

Acknowledgments

I wish to thank Dr. Rabi Mehta, of the Joint Institute for Aeronautics and Acoustics, Stanford University for his considerable assistance during this project. The facilities used for this study were provided by the Fluid Dynamics Research Branch, NASA Ames Research Center.

REFERENCES

BELL, J. H. 1989 An Experimental Study of Secondary Vortex Structure in Mixing Layers. *CTR Annual Research Briefs - 1989.* Center for Turbulence Research, Stanford University, 59-79.

BELL, J. H. & MEHTA, R. D. 1989a Design and Calibration of the Mixing Layer Wind Tunnel. *JIAA Report TR-89.* Dept. of Aero/Astro, Stanford University.

BELL, J. H. & MEHTA, R. D. 1989b Three-Dimensional Structure of Plane Mixing Layers. *JIAA Report TR-90.* Dept. of Aero/Astro, Stanford University.

BELL, J. H. & MEHTA, R. D. 1990a Development of a Two-Stream Mixing Layer From Tripped and Untripped Boundary Layers. *AIAA Paper 90-0505.*

BELL, J. H. & MEHTA, R. D. 1990b Effects of Streamwise Vorticity Injection on Turbulent Mixing Layer Development. *AIAA Paper 90-1459.*

BERNAL, L. P. & ROSHKO, A. 1986 Streamwise Vortex Structure in Plane Mixing Layers. *J. Fluid Mech.* **170**, 499-525.

BROWAND, F. K. & LATIGO, B. O. 1979 Growth of the Two-Dimensional Mixing Layer from a Turbulent and Nonturbulent Boundary Layer. *Phy. Fluids.* **22**, 1011-1019.

HO, C.-M. & HUERRE, P. M. 1984 Perturbed Free Shear Layers. *Ann. Rev. Fluid Mech.* **16**, 365-424.

HUANG, L.-S. & HO, C.-M. 1990 Small-Scale Transition in a Plane Mixing Layer. *J. Fluid Mech.* **210**, 475-500.

JIMENEZ, J., COGOLLOS, M., & BERNAL, L. P. 1985 A Perspective View of the Plane Mixing Layer. *J. Fluid Mech.* **152**, 125-143.

KONRAD, J. H. 1977 An Experimental Investigation of Mixing in Two-Dimensional Turbulent Shear Flows with Applications to Diffusion-Limited Chemical Reactions. *Ph.D. Thesis.* California Institute of Technology

LASHERAS, J. C., CHO, J. S. & MAXWORTHY, T. 1986 On the Origin and Evolution of Streamwise Vortical Structures in a Plane, Free Shear Layer. *J. Fluid Mech.* **172**, 231-258.

LASHERAS, J. C. & CHOI, H. 1988 Stability of a Plane Turbulent Shear Layer to Axial Perturbations. *J. Fluid Mech.* **189**, 53-86.

MOSER, R. D., & ROGERS, M. M. 1990 Spanwise Scale Change in a Time-Developing Mixing Layer. *Bulletin of the American Physical Society.* **35**, 10, 2294.

NYGAARD, K., & GLEZER, A. 1991 Spanwise-Nonuniform Excitation of a Plane Shear Layer. *AIAA Paper 91-0625.*

ROGERS, M. M., & MOSER, R. D. 1989 The Development of Three-Dimensional Temporally-evolving Mixing Layers. *Proceedings of the 7th Symposium on Turbulent Shear Flows, Aug. 21-23, Stanford University.* **1**, 9.3.1-9.3.6.

RODI, W. 1975 In: *Studies in Convection* (ed. B. E. Launder), *vol.* 1, *pp.* 79-165, Academic Press, London.

SANDHAM, N. D., MUNGAL, M. G., BROADWELL, J. E., & REYNOLDS, W. C. 1988 Scalar Entrainment in Mixing Layers. *Proceedings of the 1988 Summer Program, Center for Turbulence Research.* **CTR-S88**, 69-76.

TOWNSEND, A. A. 1976 *Structure of Turbulent Shear Flow* (2nd Edition). *Cambridge University Press, Cambridge.*